

EINDHOVEN UNIVERSITY OF TECHNOLOGY

HAPTICS  
4SC040

---

# 1-DOF Bilateral Teleoperation Haptic Feedback Controller

Experimental Assignments

---

*Authors:*  
Linda Feenstra (0847751)  
Christopher Ohara (1322884)

June 21, 2018

# 1 Assignment 1

The objective of this assignment is to compare the position-position architecture (PP) with the position-force architecture (PF) for different sets of control parameters. Both architectures are applied on the 1-DOF Haptic Setup shown in Figure 1.

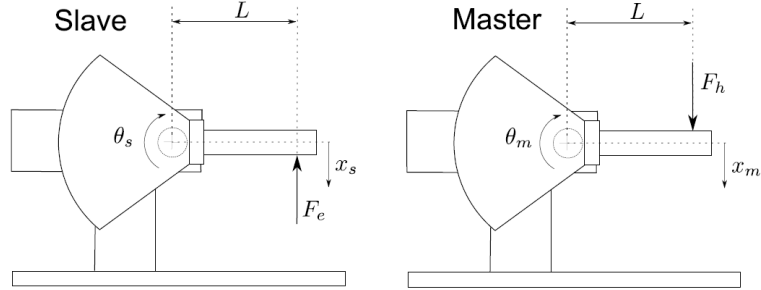


Figure 1: Bilateral teleoperator

The master device is positioned on the right side and the slave is positioned on the left. The orientation of the beams, i.e.  $q_m$  and  $q_s$  respectively, and the torques  $\tau_h$  and  $\tau_e$ , resulting from applied forces on the end-effectors, are measured and can be used in the control architectures. Noisy force signals are filtered with a low-pass filter with a cut-off frequency of 25 Hz for  $\tau_h$  and 40 Hz for  $\tau_e$ . Velocity signals are obtained from the orientation measurements by numerical differentiation and the use of a low-pass filter with a cut-off frequency of 100 Hz. The transfer functions from control torque  $\tau_i$  to rotation  $\theta_i$ ,  $i \in \{m; s\}$ , of both master and slave are shown in Figure 2, together with the coherence of the sensitivity, obtained from the data of the identification measurements from the zip-file 1DOF\_measurements.

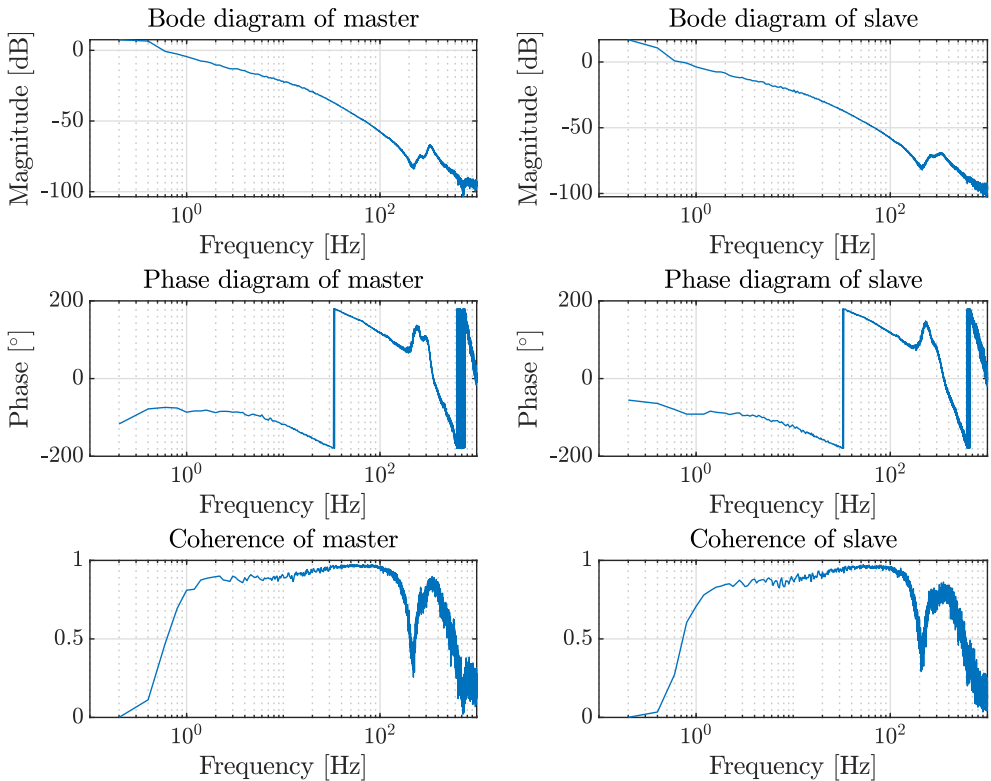


Figure 2: Frequency response measurements 1DOF Haptic Setup

a) The following PP-controller is joint space is considered:

$$\begin{aligned}\tau_{mc}(t) &= K_p[\theta_s(t) - \theta_m(t)] + K_d[\dot{\theta}_s(t) - \dot{\theta}_m(t)] \\ \tau_{sc}(t) &= K_p[\theta_m(t) - \theta_s(t)] + K_d[\dot{\theta}_m(t) - \dot{\theta}_s(t)]\end{aligned}$$

with  $K_p = 8$  and  $K_d = 0.1$ . The control structure is selected in Simulink by selecting the controller position-position. The bandwidth of the open loop system can be interpreted as the frequency where the open loop frequency response function first crosses 0 dB.

The position controller is tested in free motion and in contact with three test objects: the aluminum cylinder with a spring ( $k_e \approx 400$  N/m), the aluminum cylinder with foam ( $k_e \approx 4000$  N/m) and the solid aluminum cylinder.

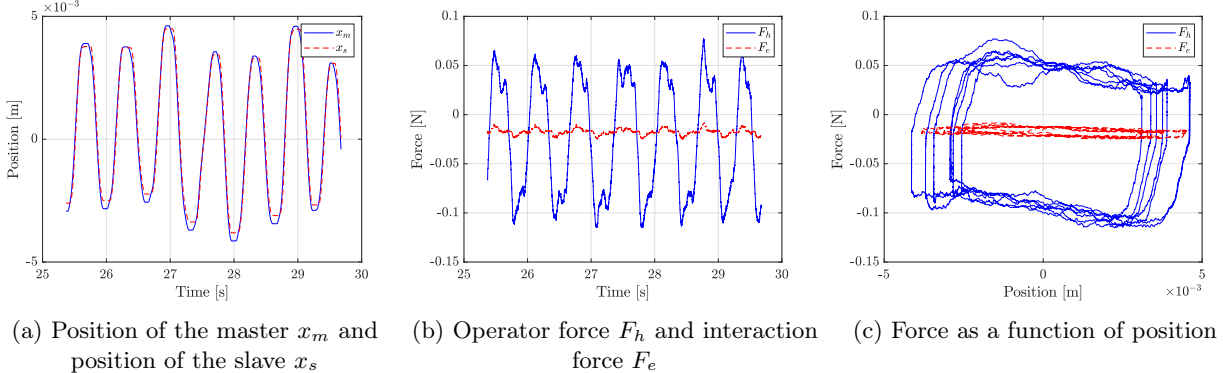


Figure 3: Experiment of the PP-controlled teleoperator for free motion

Figure 3 shows an experiment with the PP-controller in free-motion. As can be seen in Figure 3a the slave follows the position of the master very well, especially during constant velocity intervals. Figure 3b points out that the operator force  $F_h$  is much larger than the interaction force of the slave with the environment  $F_e$ .  $F_e$  is very small. In Figure 3c it can be seen that the stiffness perception is acceptable, since the average slopes of  $F_h$  and  $F_e$  versus position are approximately the same. Little damping is felt by the slave and more damping is felt by the master.

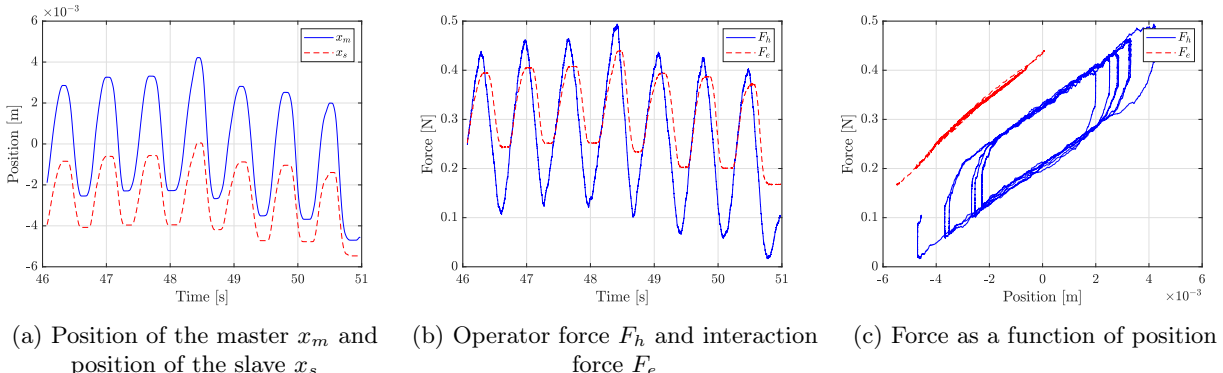


Figure 4: Experiment of the PP-controlled teleoperator for the aluminum cylinder with spring ( $k_e \approx 400$  N/m)

In Figure 4 the experiment with the same PP-controller is shown, but now with the aluminum cylinder. Looking at Figure 4a it can be seen that the slave is able to follow a similar movement as the master, but the position has a certain offset created due to the stiffness of the spring that is hard to overcome. Compared to the free motion in Figure 3a the motion synchronization of Figure 4a is a lot worse by introducing the spring. The slave is unable to reach the same positions in especially the positive direction as the master. In Figure 4b it can be seen that the interaction force with the environment has considerably increased in comparison to Figure 3b for free motion.  $F_e$  is nearly as large as  $F_h$  when the manipulator moves in positive direction, so towards the spring, where the slave feels the force that the spring exerts. This force  $F_e$  increases when the spring is pushed further down. Logically, when moving away from the spring  $F_e$  is smaller, but still higher than during free motion in

Figure 3b. The stiffness perception can be read from Figure 4c which is good as the average slopes of  $F_h$  and  $F_e$  versus position are almost the same. Comparing the slopes in 4c with 3c it can be seen that the slope has increased when introducing the spring which implies a higher stiffness as expected. Very little damping is felt by the slave and more damping is felt by the master. Less damping is perceived by the master in comparison to free motion in Figure 3c.

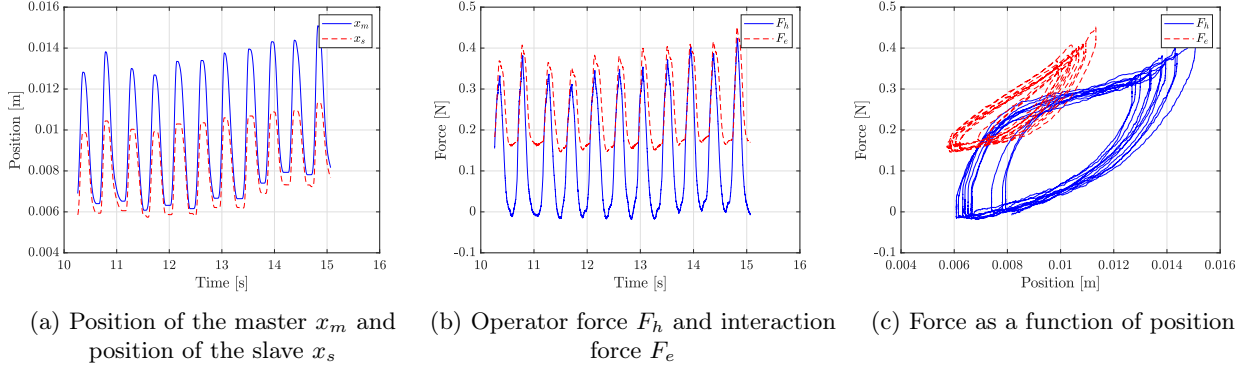


Figure 5: Experiment of the PP-controlled teleoperator for the aluminum cylinder with foam ( $k_e \approx 4000 \text{ N/m}$ )

In Figure 5 the results are shown for the experiment with the same PP-controller but now with the cylinder with foam. It is noticed from Figure 5a that the slave is able to follow the motion of the master quite well while moving in the negative direction, but it is unable to follow the master's motion during movement in the positive direction, because the stiffness of the foam is preventing this.  $F_e$  slightly larger in amplitude than  $F_h$  when the manipulator moves in positive direction, so towards the foam, where the slave feels the force that the foam exerts on it. This force  $F_e$  increases when the slave is pushed further down into the foam. Logically, when moving away from the foam  $F_e$  is smaller, but still higher then during free motion in Figure 3b. The stiffness perception is obtained from Figure 5c which is acceptable as the average slopes of  $F_h$  and  $F_e$  versus position are almost the same. Comparing the slopes in 5c with 3c it can be seen that the slope has increased when introducing the foam which implies a higher stiffness as expected. Less damping is perceived by the master in comparison to free motion in Figure 3c, but more damping than with the spring in Figure 4c. The slave also perceives a little damping.

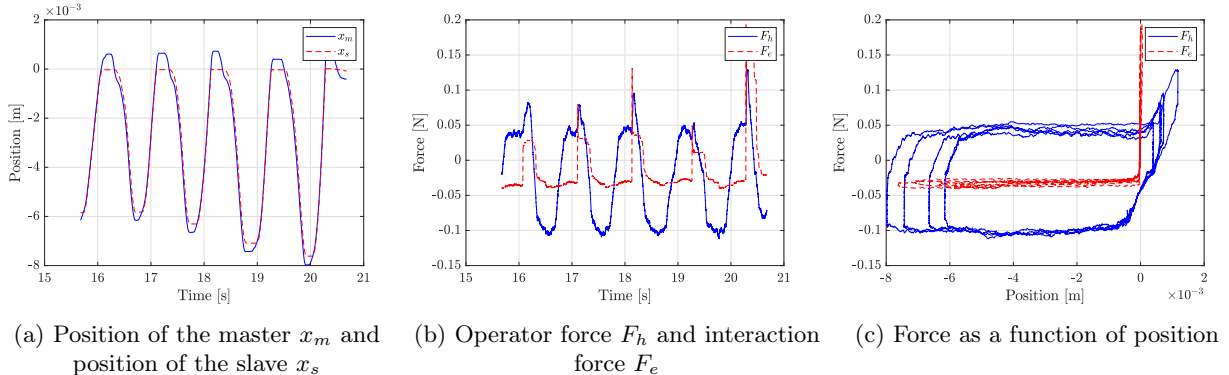


Figure 6: Experiment of the PP-controlled teleoperator for the solid aluminum cylinder

Lastly, the same PP-controller is applied but now in combination with a solid aluminum cylinder. From Figure 6a the switch between free motion and touching the solid cylinder can be seen. During free motion while the position is negative, the slave is able to follow the movement of the master well, however when reaching position 0 m it is visible that the slave comes to a stop and cannot move further, whereas the master obtains a position above 0 m. In Figure 6b is illustrated that a dirac-delta-function-like peak value in  $F_e$  is obtained when gently hitting the solid cylinder. In addition,  $F_e$  increases when the slave is pushed further down onto the solid cylinder. When moving away  $F_e$  drops. In Figure 6c the switching between free motion and touching the solid cylinder is visible more obviously, as the horizontal slope of  $F_e$  represents free motion and the steep and nearly vertical slope represents the stiffness of the solid cylinder. The stiffness perception of the cylinder is reasonably well, but it is difficult to be able to obtain a average slope that represents only data from touching the solid

cylinder. A very similar stiffness perception to Figure 3c is seen for the free motion part with the same amount of damping. Little damping is felt by the slave and more damping is felt by the master, especially during free motion.

b) Subsequently, the PP-controller is tested with  $K_p = 15$  and  $K_d = 0.1$  for free motion and the three objects.

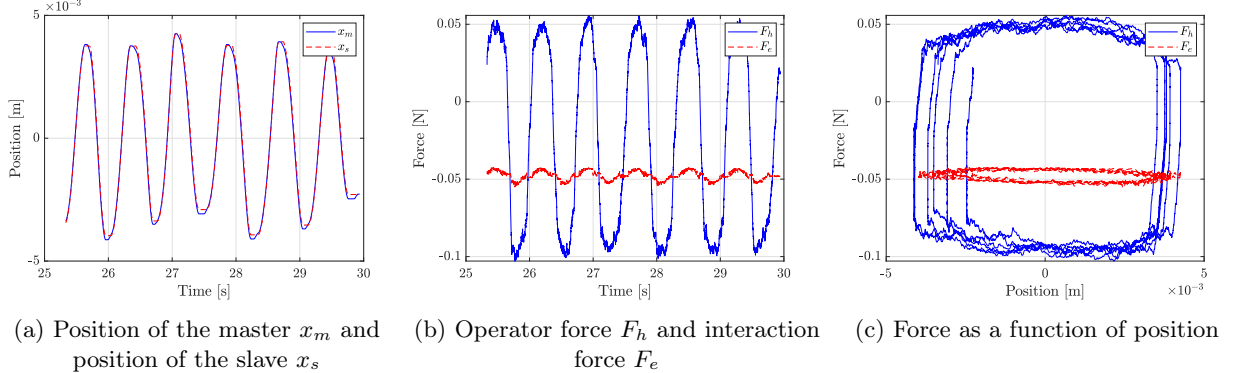


Figure 7: Experiment of the PP-controlled teleoperator for free motion

In Figure 7a is seen that for free motion the motion synchronization of the slave with the master is very good and even slightly better in comparison to the previous PP-controller Figure 3a. The operator force  $F_h$  is in amplitude very similar to the operator force from Figure 3b, however  $F_e$  has decreased by a factor 2 in comparison to 3b. Figure 7c shows the stiffness perception which is good and comparable to 3c for having about the same slopes. Furthermore, the stiffness perception obtained from Figure 7c is the same as for the previous controller in Figure 3c.

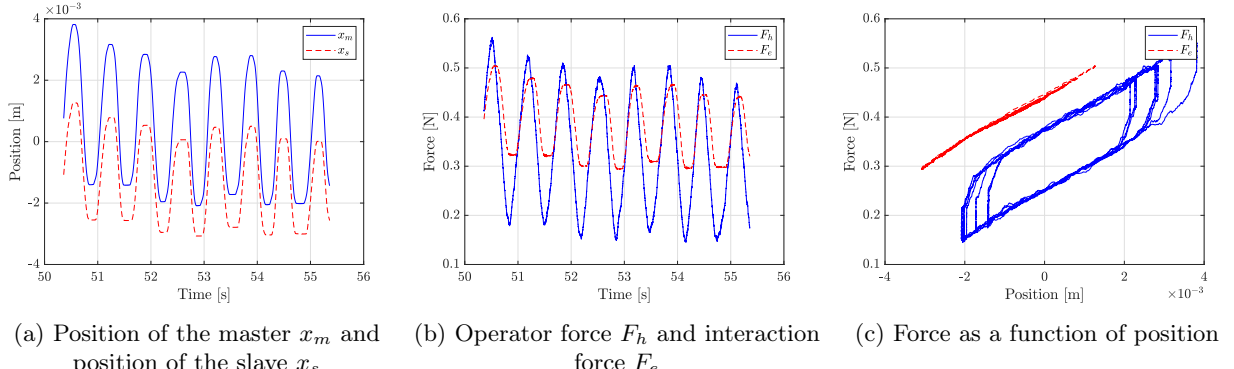


Figure 8: Experiment of the PP-controlled teleoperator for the aluminum cylinder with spring ( $k_e \approx 400 \text{ N/m}$ )

Looking at Figure 8a it is noticed that the motion synchronization is still poor compared to free motion, but it has improved somewhat in comparison to motion synchronization from the previous PP-controller in Figure 4a. The intervals of constant velocity are now a little closer to the position of the master, however the offset is still visible. The forces  $F_h$  and  $F_e$  in Figure 8b and stiffness perception are very similar to the ones in 4c from the previous PP-controller.

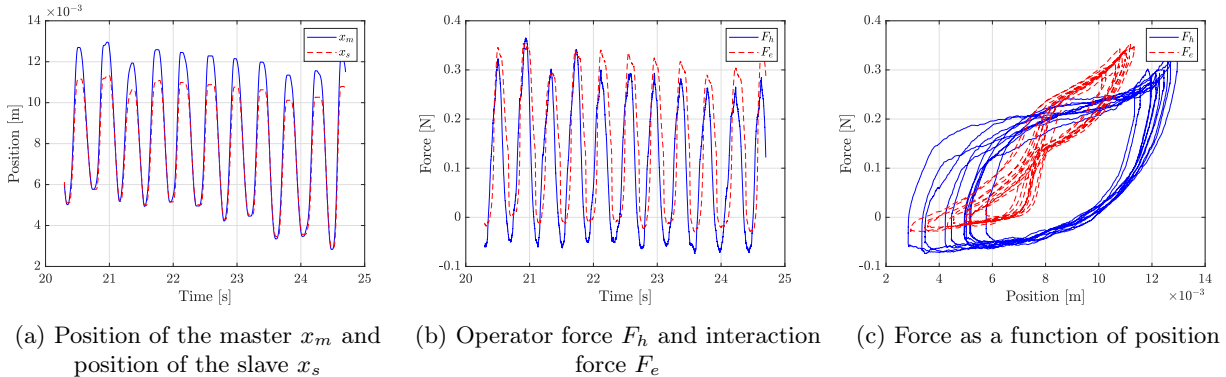


Figure 9: Experiment of the PP-controlled teleoperator for the aluminum cylinder with foam ( $k_e \approx 4000$  N/m)

In Figure 9 one can see the experiment with the second PP-controller with the aluminum cylinder with foam. The motion synchronization in Figure 9a is a little better than the motion synchronization of the previous PP-controller. This is concluded from the position of the slave that has slightly increased in positive direction towards the position of the master compared to the previous controller, in addition the turn over points are followed better and that for a overall somewhat lower operator force  $F_h$ , see Figure 9b. The stiffness perception is similar to the one in 4c from the previous PP-controller. The only thing that stands out is that the shape of  $F_e$  has transformed into a bit of a bow-tie, which indicates that for a certain position less damping is perceived by the slave.

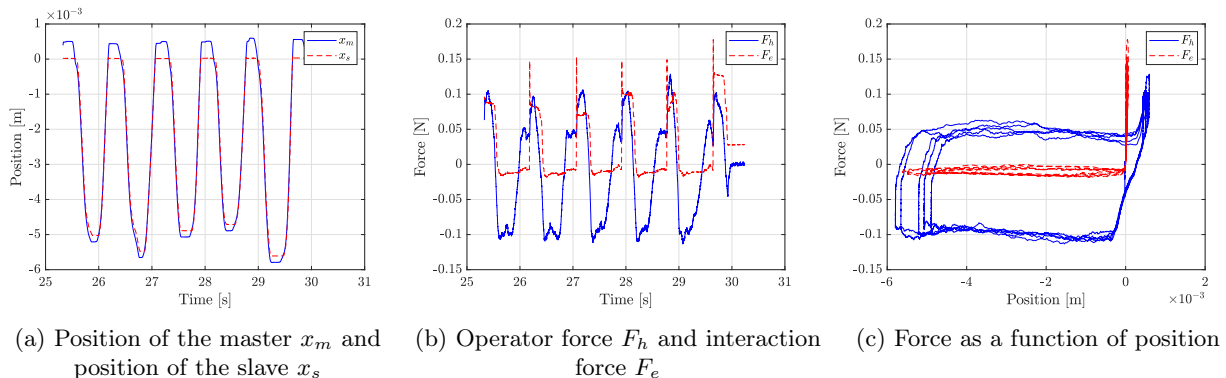
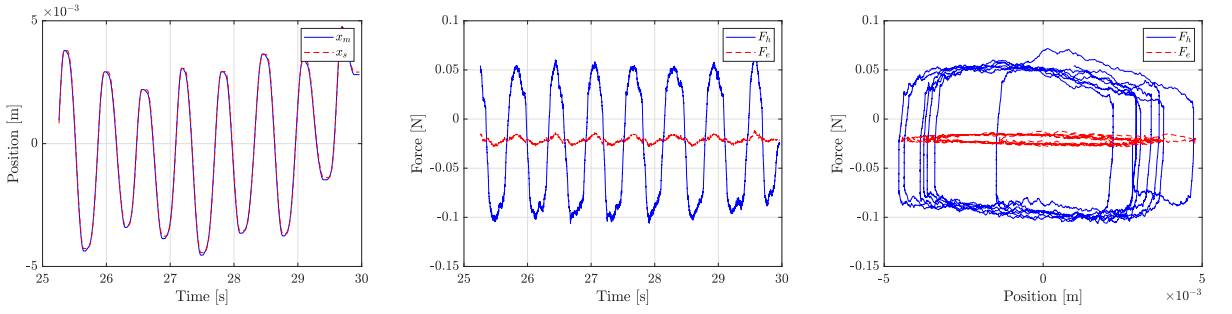


Figure 10: Experiment of the PP-controlled teleoperator for the solid aluminum cylinder

In Figure 10 very similar behavior is seen in comparison to the previous controller in Figure 6. What stands out in Figure 10b in comparison to Figure 6b is that the difference in amplitude between  $F_h$  and  $F_e$  is smaller. In addition, the stiffness of the solid cylinder is perceived a little better than for the previous controller, as the slopes in Figure 10c are more similar than in Figure 6c.

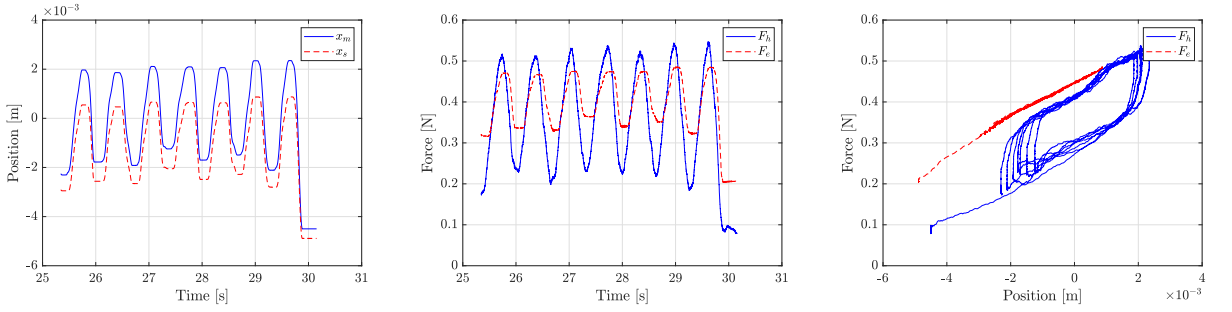
c) Next, the controller is tested with  $K_p = 25$  and  $K_d = 0.15$  for free motion and the three objects.



(a) Position of the master  $x_m$  and position of the slave  $x_s$       (b) Operator force  $F_h$  and interaction force  $F_e$       (c) Force as a function of position

Figure 11: Experiment of the PP-controlled teleoperator for free motion

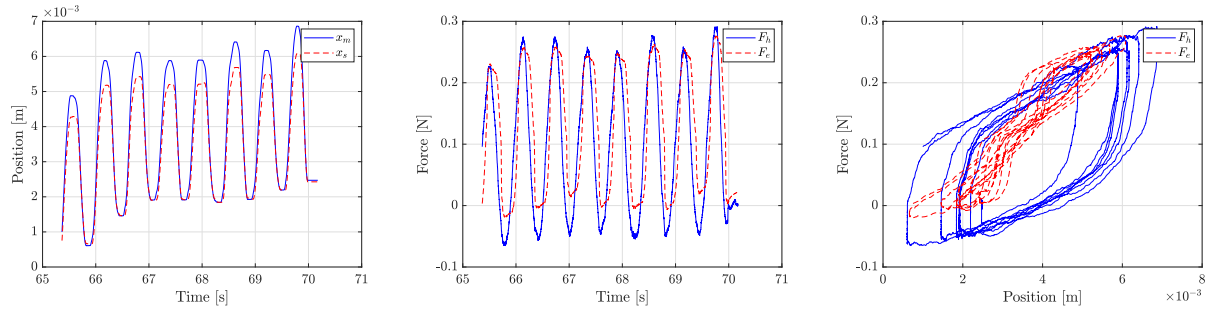
In Figure 11 one can see the experiment for the new PP-controller in free motion. In comparison to Figure 3a and 7a, the motion synchronization is in Figure 11a at its best. The error between the position of the slave and master at the turn over point seems to decrease with increasing  $K_p$ . The forces  $F_h$  and  $F_e$  illustrated in Figure 11c show most similarities with Figure 3b considering the value of  $F_e$ . Overall the behavior in Figures 3b, 7b and 11b is the same. Also the stiffness perception of 11c is most similar to Figure 3c, but very similar to both Figure 3c and 7c.



(a) Position of the master  $x_m$  and position of the slave  $x_s$       (b) Operator force  $F_h$  and interaction force  $F_e$       (c) Force as a function of position

Figure 12: Experiment of the PP-controlled teleoperator for the aluminum cylinder with spring ( $k_e \approx 400$  N/m)

The experiment with the spring for the new PP-controller is visible in Figure 12. Comparing the motion synchronization of Figure 12a with Figures 4a and 8a, it can be said that overall the motion synchronization of 12a is best for the controller with largest  $K_p$  because it has the smallest difference in position of the slave and master at the turn over point, i.e. the offset is smallest. The forces in in Figures 4b, 8b and 12b are very much the same. Also the stiffness perception of Figure 4c, 8c and 12c is very similar.



(a) Position of the master  $x_m$  and position of the slave  $x_s$       (b) Operator force  $F_h$  and interaction force  $F_e$       (c) Force as a function of position

Figure 13: Experiment of the PP-controlled teleoperator for the aluminum cylinder with foam ( $k_e \approx 4000$  N/m)

In Figure 13 the experiment with the foam is illustrated. All figures in 13 show strong similarities with the figures of Figure 9. Both Figure 9 and Figure 13 are considerably better in motion synchronization than Figure 5.

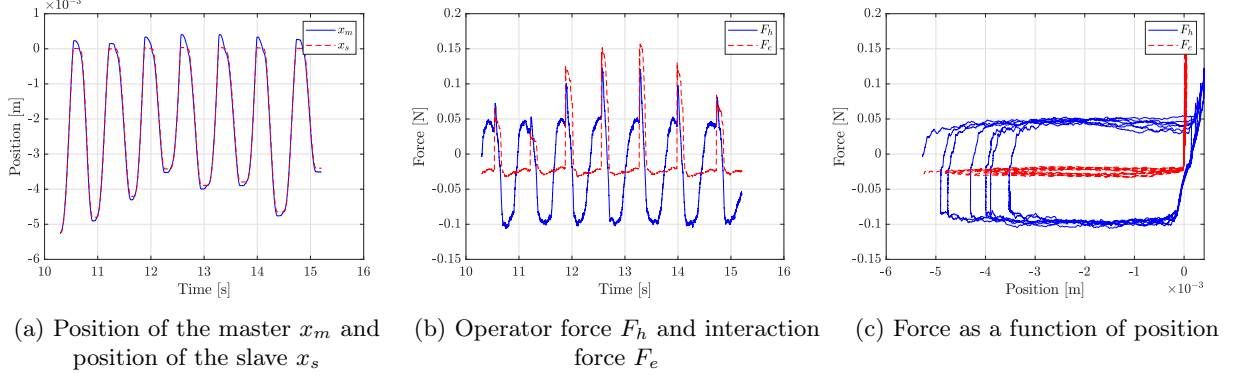


Figure 14: Experiment of the PP-controlled teleoperator for the solid aluminum cylinder

Finally, in Figure 14 the experiment with the solid aluminum cylinder is shown. The behavior is very similar to behavior in Figure 6 and 10. Figure 14b shows that in contrast to Figures 6b and 10b the difference in amplitude between  $F_h$  and  $F_e$  has become larger, except for the movements while gently hitting the solid cylinder. The stiffness perception in Figure 14c is most similar to Figure 10c, because in both Figure 10c and Figure 14c the stiffness perception looks better than in Figure 6c.

d) The following PF-controller is joint space is considered:

$$\begin{aligned}\tau_{mc}(t) &= -\tau_e(t) \\ \tau_{sc}(t) &= K_p[\theta_m(t) - \theta_s(t)] + K_d[\dot{\theta}_m(t) - \dot{\theta}_s(t)]\end{aligned}$$

with  $K_p = 8$  and  $K_d = 0.1$ . The control structure is selected in Simulink by selecting the controller position-force.

The new controller is tested in free motion and in contact with the same three test objects: the aluminum cylinder with a spring ( $k_e \approx 400$  N/m), the aluminum cylinder with foam ( $k_e \approx 4000$  N/m) and the solid aluminum cylinder.

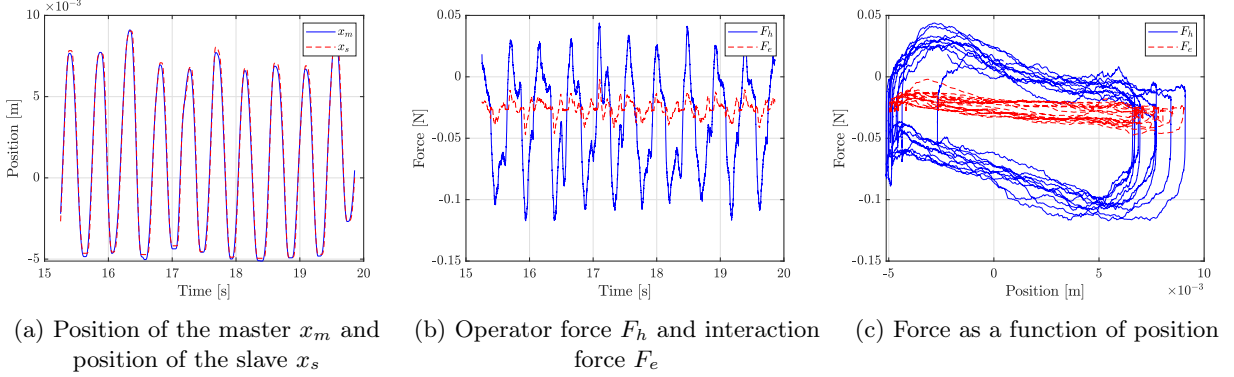
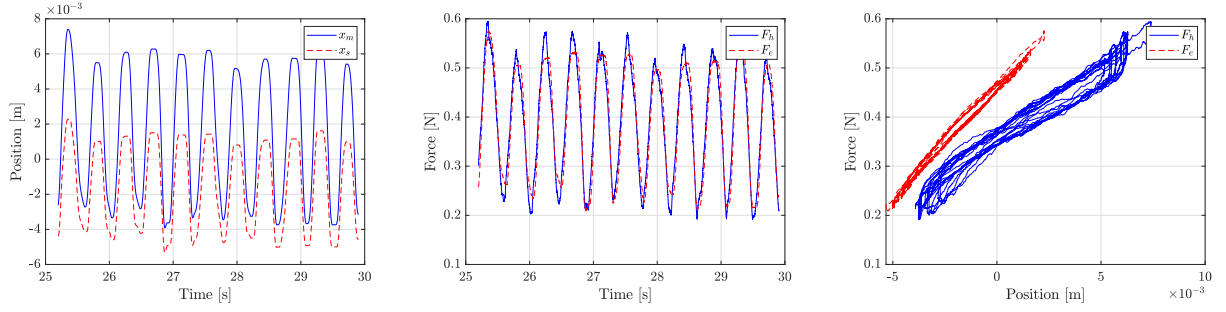


Figure 15: Experiment of the PF-controlled teleoperator for free motion

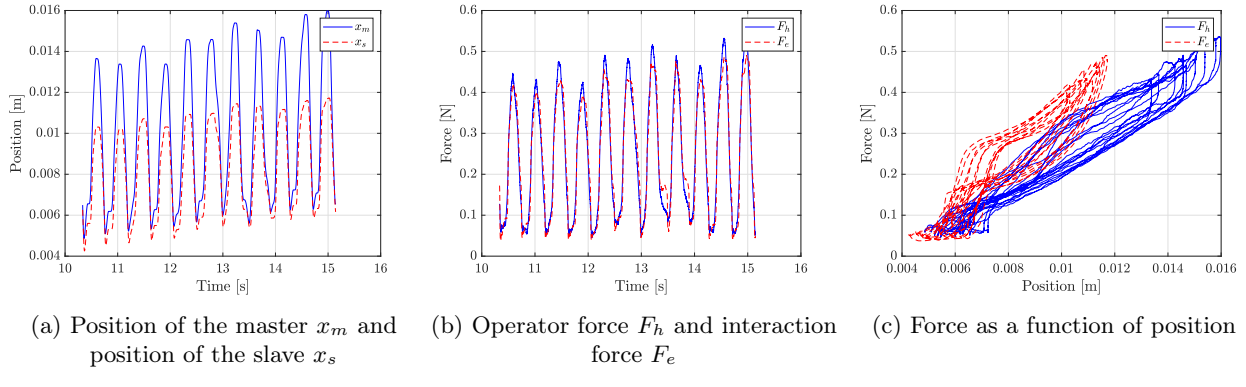
In Figure 15 the experiment with the PF-controller can be seen in free motion. Comparing this experiment with the PP-controller in Figure 3 with the same parameter values for  $K_p$  and  $K_d$  it can be seen that the motion synchronization of Figure 15a is slightly better for the PF-controller at the turn overs than for the PP-controller in Figure 3a. In addition, the forces in Figure 15b and Figure 3b are similar. The stiffness perception in Figure 15c differs from the one in Figure 3c for the slope of the master has become more negative and therefore the stiffness perception worsens.



(a) Position of the master  $x_m$  and position of the slave  $x_s$       (b) Operator force  $F_h$  and interaction force  $F_e$       (c) Force as a function of position

Figure 16: Experiment of the PF-controlled teleoperator for the aluminum cylinder with spring ( $k_e \approx 400$  N/m)

In Figure 16 the experiment with the PF-controller is shown with the spring. When the results in Figure 16b are compared with Figure 4b a large difference can be seen using the PF-controller. In Figure 16b the forces  $F_e$  and  $F_h$  are almost the same during the entire movement, whereas in Figure 4b the forces  $F_e$  and  $F_h$  are not the same where the position is negative. In addition, less damping is perceived by the master according to Figure 16c in comparison with Figure 4c.



(a) Position of the master  $x_m$  and position of the slave  $x_s$       (b) Operator force  $F_h$  and interaction force  $F_e$       (c) Force as a function of position

Figure 17: Experiment of the PF-controlled teleoperator for the aluminum cylinder with foam ( $k_e \approx 4000$  N/m)

In Figure 17 the experiment for the PF-controller is shown using the foam. Again, the same two things are obvious when Figure 17 is compared to Figure 5. In Figure 17b the forces  $F_e$  and  $F_h$  are almost the same during the entire movement, whereas in Figure 5b the forces  $F_e$  and  $F_h$  are not the same where the position is negative. In addition, less damping is perceived by the master according to Figure 17c in comparison with Figure 5c.

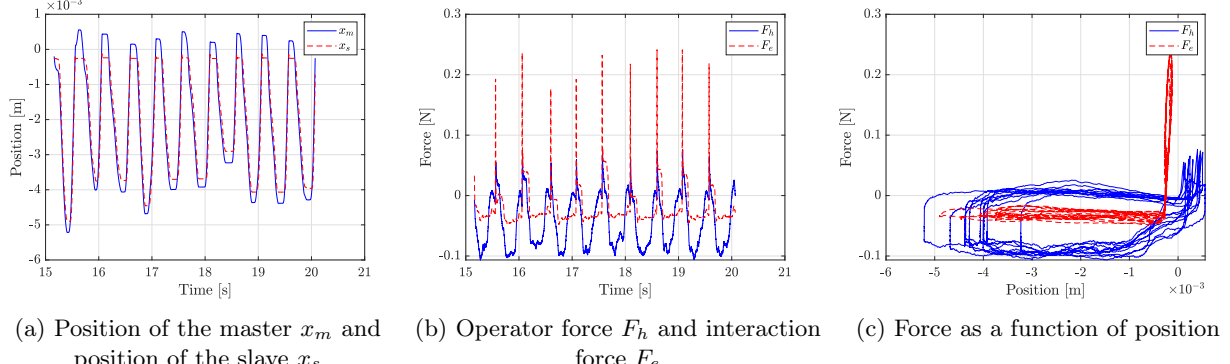


Figure 18: Experiment of the PF-controlled teleoperator for the solid aluminum cylinder

The experiment with the solid cylinder for the PF-controller is shown in Figure 18. Very similar results are

obtained when compared to the PP-controller with the same parameters values for  $K_p$  and  $K_d$  in Figure 6. The largest difference between the two controller is visible in Figure 18b where the dirac-delta-function-like peak values of  $F_e$  are a lot higher than the peak values of  $F_h$  in contrast to Figure 6b where the peak values of  $F_e$  are  $F_h$  are comparable.

e) Next, the PF-controller is tested with  $K_p = 15$  and  $K_d = 0.1$  for free motion and the three objects.

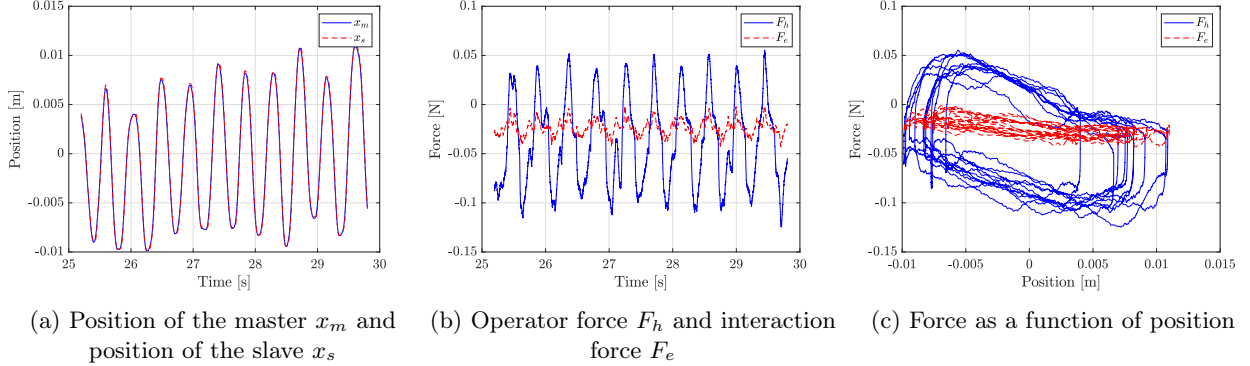


Figure 19: Experiment of the PF-controlled teleoperator for free motion

In Figure 19 the behavior is shown for the new PF-controller in free motion. Compared to the PP-controller with the same values for  $K_p$  and  $K_d$  the motion synchronization has improved at the turn over points, see Figure 19a.  $F_e$  also has a larger amplitude using the PF-controller in comparison to the PP-controller. Furthermore, compared to the PP-controller, the stiffness perception using PF-controller has changed a bit for the slope of the master has become more negative and therefore the stiffness perception worsens. No obvious differences are seen comparing the current PF-controller in Figure 19 with the older one in Figure 15.

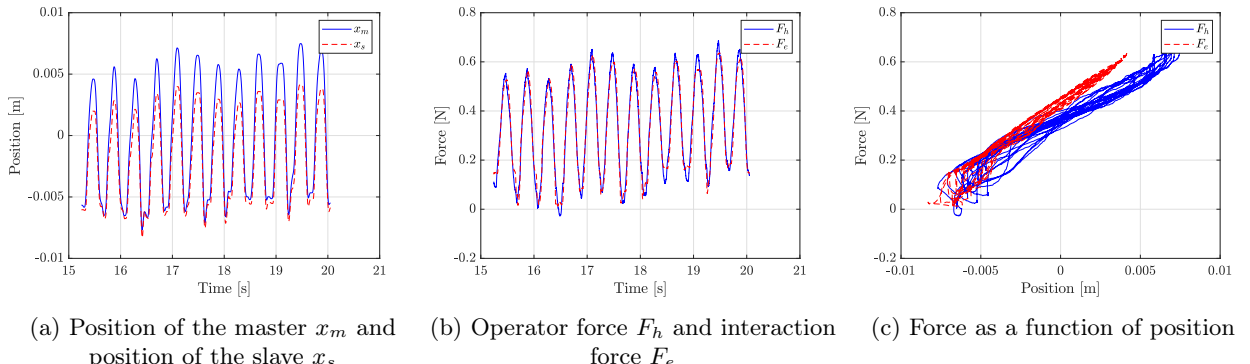
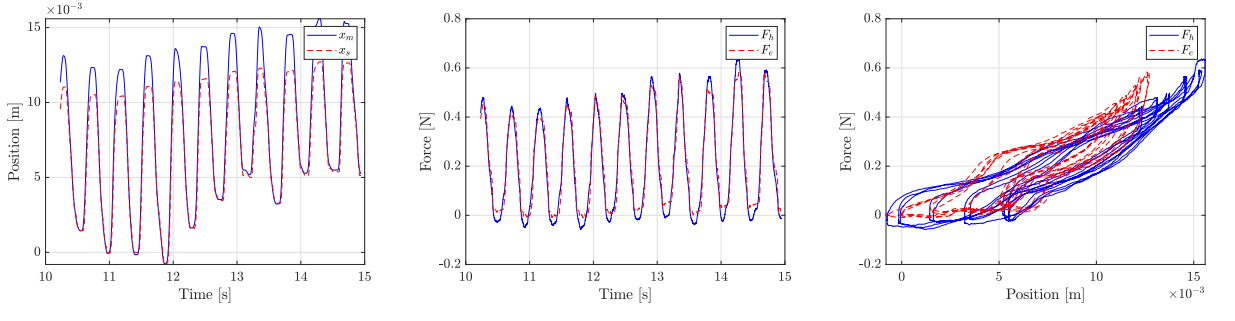


Figure 20: Experiment of the PF-controlled teleoperator for the aluminum cylinder with spring ( $k_e \approx 400$  N/m)

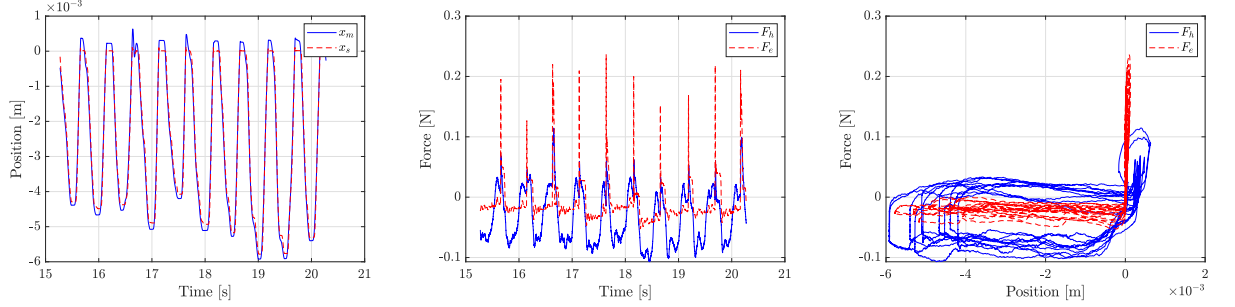
Figure 20 shows the experiment with the PF-controller in combination with the spring. Compared to the PP-controller with the same values for  $K_p$  and  $K_d$  the motion synchronization has improved a lot, see Figure 20a. In addition, in Figure 20b  $F_e$  and  $F_h$  have approximately the same amplitude, whereas in Figure 8b they have not. The master in Figure 20c perceives less damping compared to Figure 8c. Comparing Figures 20 and 16 it can be said that they are similar to a great extent. Motion synchronization seems somewhat better at the turn over points in Figure 20a.



(a) Position of the master  $x_m$  and position of the slave  $x_s$       (b) Operator force  $F_h$  and interaction force  $F_e$       (c) Force as a function of position

Figure 21: Experiment of the PF-controlled teleoperator for the aluminum cylinder with foam ( $k_e \approx 4000$  N/m)

Figure 21 the experiment with the PF-controller in combination with the foam is illustrated. Compared to the PP-controller with the same values for  $K_p$  and  $K_d$  the motion synchronization is similar.  $F_e$  and  $F_h$  have approximately the same amplitude in both Figure 21b and 9b, but in Figure 9b  $F_e$  is slightly larger than  $F_h$ . The master in Figure 21c perceives less damping compared to Figure 9c. Comparing Figures 21 and 17 it can be said that they are similar to a great extent. Motion synchronization seems somewhat better at the turn over points in Figure 21a.



(a) Position of the master  $x_m$  and position of the slave  $x_s$       (b) Operator force  $F_h$  and interaction force  $F_e$       (c) Force as a function of position

Figure 22: Experiment of the PF-controlled teleoperator for the solid aluminum cylinder

In Figure 22 the experiment with the PF-controller is shown for the solid cylinder. When the results are compared to the results for the PP-controller with the same parameter values for  $K_p$  and  $K_d$  no large differences are seen. The largest difference between the two controllers is visible in Figure 22b where the dirac-delta-function-like peak values of  $F_e$  are a lot higher than the peak values of  $F_h$  in contrast to Figure 10b where the peak values of  $F_e$  are  $F_h$  are comparable. When comparing Figures 22 and 18, it can be seen that the motion synchronization in Figure 22 is slightly better.

f) Now, the PF-controller is tested with  $K_p = 25$  and  $K_d = 0.15$  for free motion and the three objects.

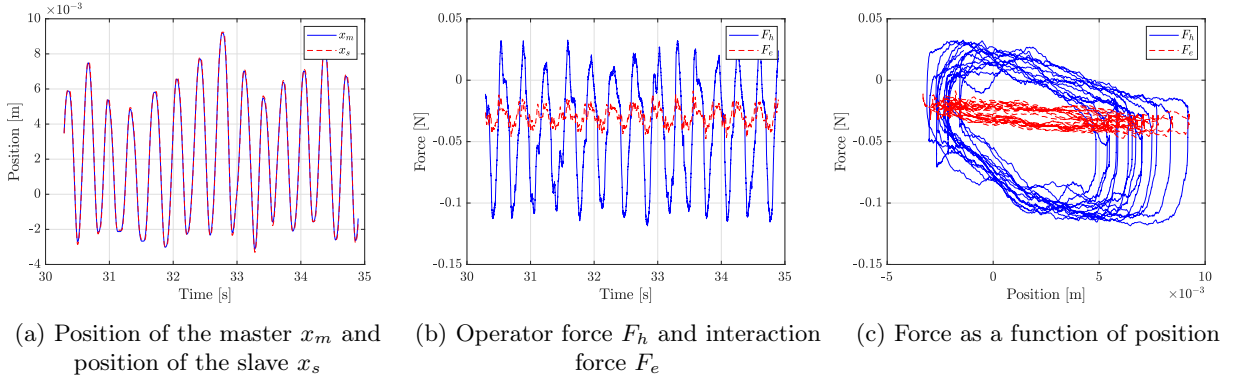


Figure 23: Experiment of the PF-controlled teleoperator for free motion

In Figure 23 the experiment with the PF-controller for free motion is shown. The motion synchronization of Figures 11a, 15a, 19a and 23a are all quite well. Also the forces and the stiffness reflections are all quite the same, with the exception that the  $F_h$  in Figure 11c has a less negative slope compared to the others.

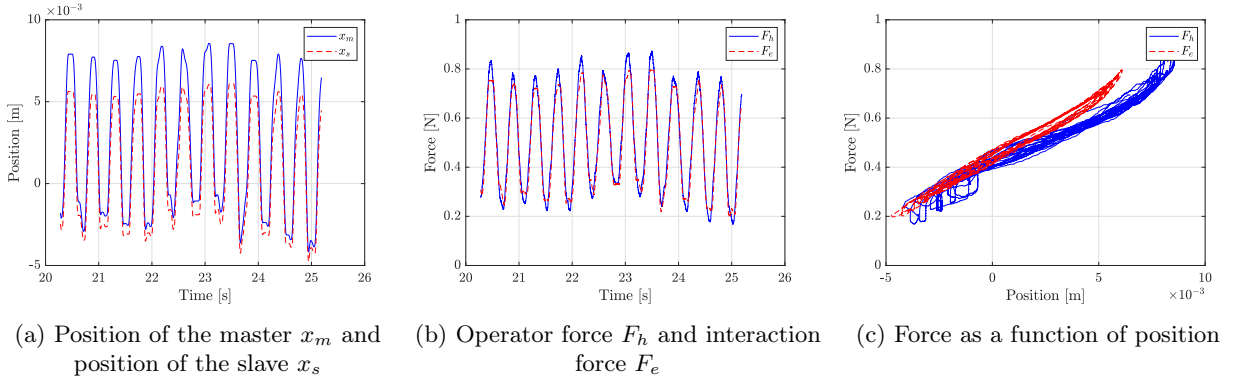


Figure 24: Experiment of the PF-controlled teleoperator for the aluminum cylinder with spring ( $k_e \approx 400$  N/m)

In Figure 24 the experiment with the PF-controller using the spring is shown. Motion synchronization in Figure 24a is comparable with Figure 20a and improved a lot compared to Figure 12a and Figure 16a. The forces look alike in Figures 16b, 20b and 24b and are of the same amplitude in contrast with 12b. The stiffness perceptions of Figures 20c and 24c are mostly the same in contrast with 12c where the damping the master perceives is higher. The stiffness perception of Figure 16c is the worst, the others are comparable.

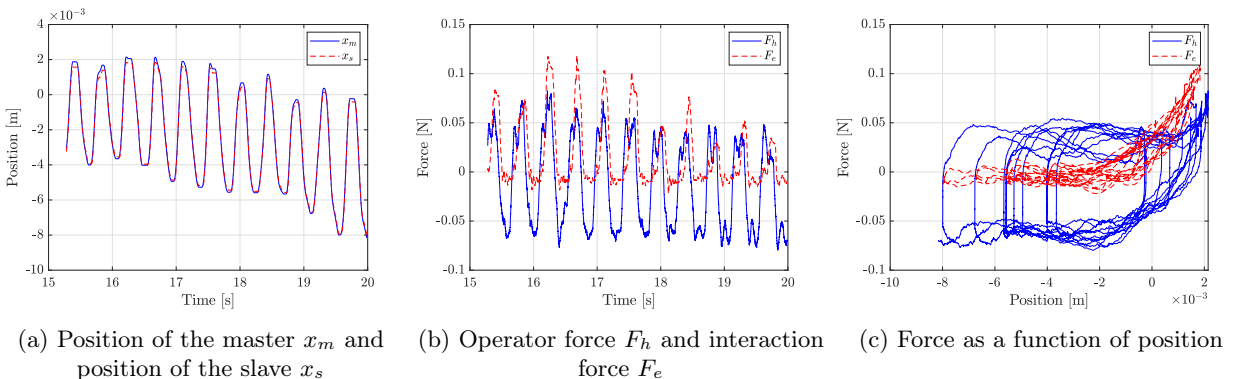


Figure 25: Experiment of the PF-controlled teleoperator for the aluminum cylinder with foam ( $k_e \approx 4000$  N/m)

In Figure 25 the experiment with the PF-controller using the foam is shown. Motion synchronization in Figure 25b is best compared to 13b, 17b and 21b, although this could be the cause of the lower amplitude. The force

$F_e$  in Figure 25b is very different from 13b, 17b and 21b where  $F_e$  and  $F_h$  are of the same amplitude. Yet again this could be caused by the fact that only  $F_e$  in Figure 25b goes below 0 m.

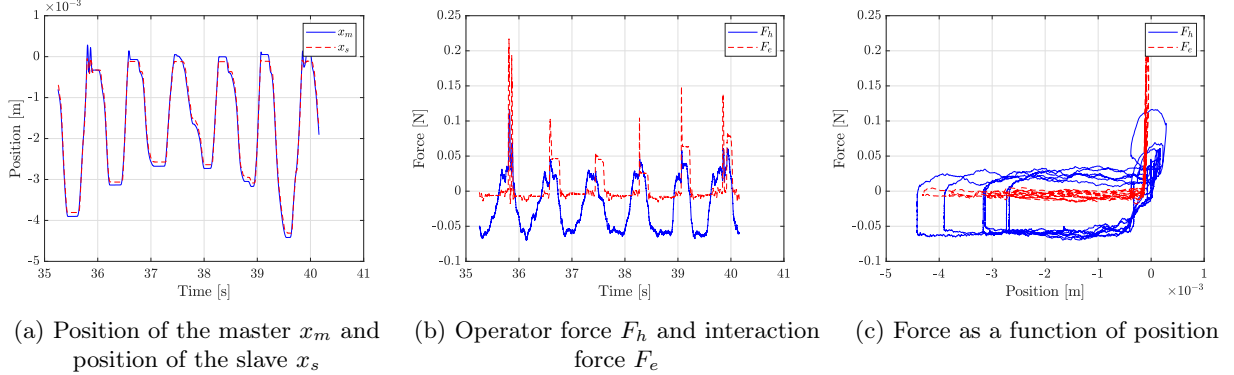


Figure 26: Experiment of the PF-controlled teleoperator for the solid aluminum cylinder

In Figure 26 the experiment with the PF-controller using the solid cylinder is shown. Motion synchronization in Figure 26b is best compared to 14b, 18b and 22b. The force  $F_e$  in Figures 18b, 22b and 26b shown similar behavior. Only the peaks in  $F_e$  in Figure 14b are smaller. The stiffness perception of the solid cylinder has worsened compared to Figures 14c, 18c and 22c, as the slope of  $F_h$  diverges ad bit from the slope of  $F_e$ , see Figure 26c.

g) The controller that is recommended for free motion for the slave is a PP-controller with  $K_p = 25$  and  $K_d = 0.15$  since this gives compared to the other parameter values for  $K_p$  and  $K_d$  the best results for motion synchronization. Furthermore, PP is preferred over PF in this case since the stiffness perception for the PP-controller is better. The best controller for the detection of the spring is a PF-controller with  $K_p = 25$  and  $K_d = 0.15$ , since motion synchronization is better than with PP-control and the forces  $F_e$  and  $F_h$  are alike. The best controller for the detection of the foam is PF with  $K_p = 15$  and  $K_d = 0.1$ , since the motion synchronization is good, forces  $F_e$  and  $F_h$  are alike and stiffness perception is well. Finally, the best controller for the detection of the solid cylinder is PF with  $K_p = 15$  and  $K_d = 0.1$ , since it has a good stiffness reflection and the motion synchronization is fine.

h) A delay would cause the position of the slave to lack behind. This would work through into the forces that the master perceives from the slaves which are actually from a time instance ago. A delay could more easily cause oscillations and instability this way, especially with high gains. A common solution for PP-control with delay is to inject damping. Bilateral motion synchronization (PP-control) architectures suffer from delay-induced forces. A solution would be to lower the  $K_p$ , but a downside is that the reflected stiffness also lowers. Also for PF-control it is recommended to inject damping.

## 2 Assignment 2

### 2.1 Haptic Feedback Controller Design for Ocular Surgery

The task is to simulate and analyze the environment in which an occluded vein is causing partial blindness in a patient. The haptic controller system is designed to allow the user operate a controller from a remote master location in order to allow the slave robot remove the obstruction with a specialized needle. The needle can only be equipped with either a distance or a force sensor. While eyes have similar dimensions, precision is absolutely required to avoid unnecessary damage.

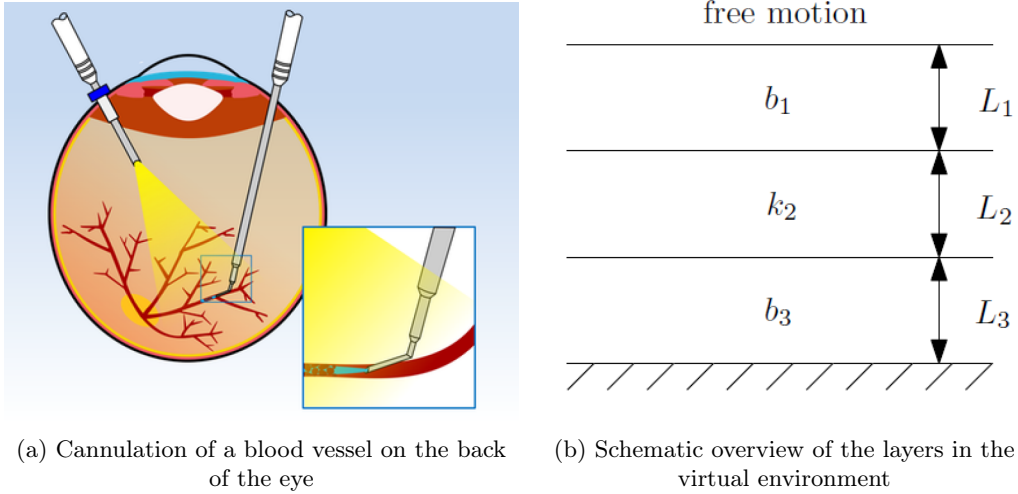


Figure 27: Virtual environment for telemanipulation task in eye surgery

### 2.2 Controller Design

The controller is made according to the PF-architecture:

$$\begin{aligned}\tau_{mc}(t) &= -\tau_e(t) \\ \tau_{sc}(t) &= K_p[\theta_m(t) - \theta_s(t)] + K_d[\dot{\theta}_m(t) - \dot{\theta}_s(t)]\end{aligned}$$

where  $\tau_e = F_{virt\_env}L$  and  $L = 0.075$  is the length of the arm of the manipulator.

The controller was altered by implementing the changes in the Simulink file. An input from the  $F\_e$  virtual was added to the master controller, followed by an input of the arm length,  $L = -0.075$ . This input is added to the contribution of the Low-pass filter and the gain is increased to  $K_p = 20$ .

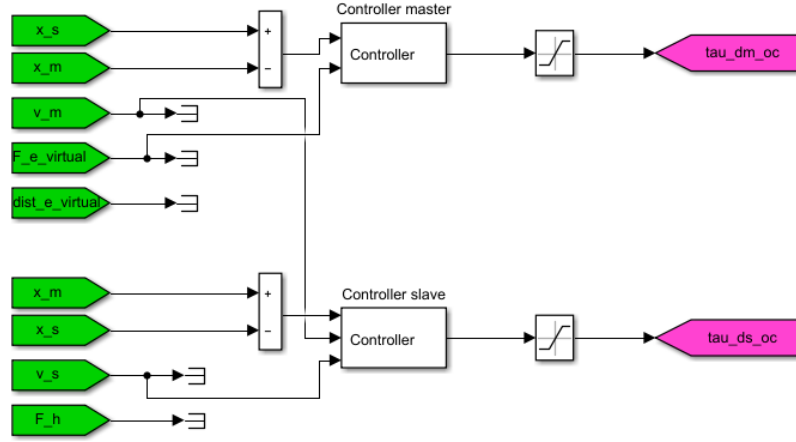
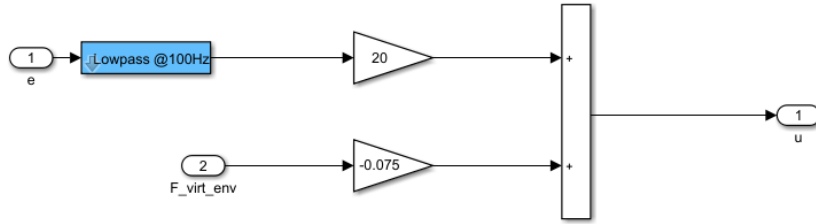
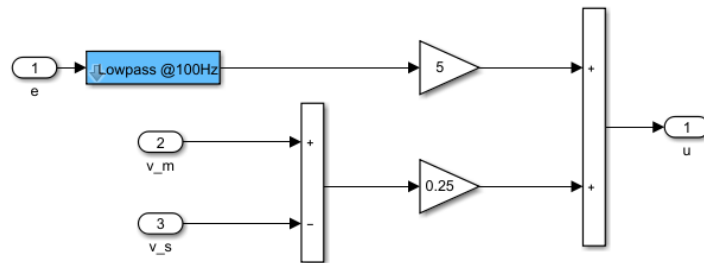


Figure 28: Structure of the controller



(a) Controller master



(b) Controller slave

Figure 29: Virtual environment for telemanipulation task in eye surgery

The master controller consists of the already implemented low pass at 100 Hz with a gain of  $K_p = 20$ , and in addition  $-\tau_e$ .

The slave controller consists of the already implemented low pass at 100 Hz with a gain of  $K_p = 5$ , and in addition some derivative action with  $K_d = 0.25$ .

Resistance is felt at the point of entering layer  $L_1$  and reaching the end of layer  $L_3$ .

## 2.3 Parameter Design Approaches

Various design parameters were explored, including:

- Scaling the distance between master and slave robot operations
- Adjusting the stiffness felt in the master robot
- Attempting to rely only on the distance value
- Attempting to rely only on force feedback (stiffness)

The goal of scaling the movements between the master and slave controllers was intended for allowing the operator to move large distances while the slave moved slightly. Experiments were conducted where the master moved at  $4x$ ,  $2x$ ,  $1x$ ,  $\frac{1}{2}x$ , and  $\frac{1}{4}x$  the slave's distance. However, a 1:1 had the best results in practice, as it was the most intuitive for the researchers. Having the ability to make larger movements can allow for surgeons to be able to make larger movements without causing tools (the needle in this case) from causing undesired damage and increases control. However, due to the rotational component of the 1-DOF controllers, a 1:1 improved the expected movement behavior of the slave controller, which prevented embedding the needle too deeply into the patient's eye.

Adjusting the perceived stiffness in the master controller was explored in order to safely move the needle without damaging the patient. Since there is a small delay in communication, the threshold  $x_{\text{target}}$  value could accidentally be exceeded. The gain was increased by ratios of  $K_p : K_d$  between the ranges of  $K_p : K_d \in (1, 70)$  for the slave controller. For the master controller,  $K_p$  was increased from values between  $K_p \in (1, 40)$ . When the ratio is lower than  $K_p : K_d = 10 : 1$ , the resistivity was too low for stable performance. When the ratio exceeded  $K_p : K_d = 50 : 1$ , the stiffness made the controller very difficult to operate and added jitter to the movements in the slave.

Next, while adjusting the  $K_p : K_d$  ratio, tests were conducted to analyze the impacts of removing all force feedback and relying only on distance. Without the force feedback, the transition states between the layers of the eye could not be felt, which required the operator to focus on the value of  $x_{\text{target}}$  more intently. Simultaneously, without the force feedback, the controller was less stable which often results in a "oscillating" behavior, as the needle might slowly retract back into the eye.

A more theoretical experiment also took place, in which the researchers attempt to rely only on force feedback. When the slave controller is tuned such that the gain is between 20x and 40x, the transitions between layers can distinctly be felt. A small jerk can be felt when entering  $L_1$  from free motion and an increase in effort is required at  $L_2$  and  $L_3$ . However, relying on only force feedback is not sufficient in knowing the absolute distance and occasionally the researches could not distinguish the difference between layers once the first layer had been breached, when conducting the experiment without relying on visual feedback.

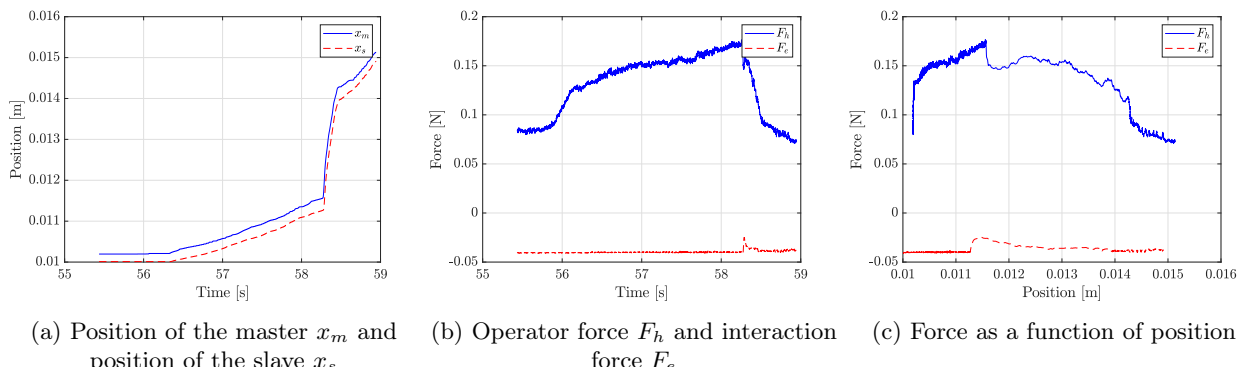


Figure 30: Capturing the transition point between free motion and  $L_1$  with own controller.

## 2.4 Parameter Selection Based on Preference

Two different researches were involved in discussing which parameters were "optimal". One researcher preferred to have more stiffness reflection with a high gain ratio ( $K_p : K_d = 40 : 1$ ) so that more accurate movements could be acquired. The other researcher preferred less stiffness ( $K_p : K_d = 20 : 1$ ), as the arm was easier to move and reflected a "smoother" feeling. This contrast leads to quite different gain selections and controller design. The closest attempt at reaching the maximum depth came to a value of 0.004998, where the damage distance was 0.005000 when using  $K_p : K_d = 40 : 1$  for the slave controller and  $K_p = 20$  for the master controller.

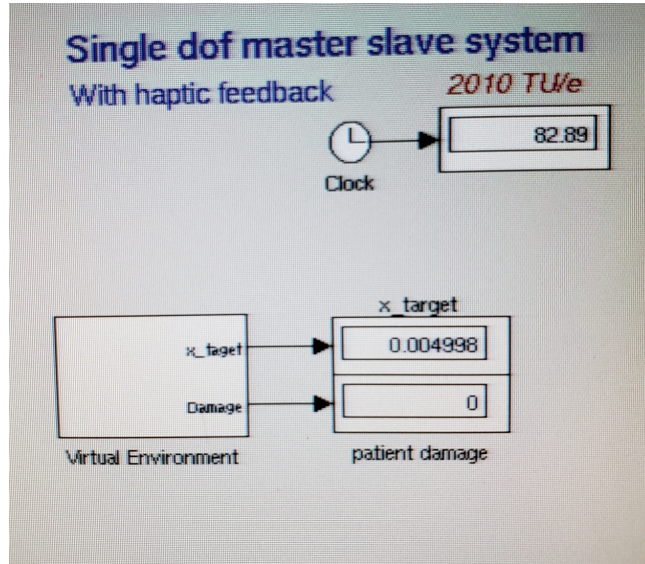


Figure 31: Approaching absolute threshold (at  $x = 0.005$ ) distance inside eye.

With this in mind, it is important to design haptic feedback devices with "variable control" or a pre-selection of ranges (like a varistor for feedback). Keeping stakeholders' preferences in mind will determine how successful wide-scale implementation will be. Similarly, performance is also an inverse function of the reflected stiffness of haptic feedback. Users' should be informed that, with current solutions, trade-offs are inevitable between performance, accuracy, and haptic feedback.

Another benefit to a high resistivity is that the needle will relatively stay in place if the user reduces their force. This is different when the master robot is easier to move, as the needle can "jerk back" when force is removed or reduced. This could lead to potentially permanent damage, if the needle is arbitrarily moving around inside the eye. In the event the procedure was not completed, it would also likely require the entire procedure to be restarted which results in another hole in the eyeball. Implementing an additional controller that can "save the state" of the needles' position (like discussed in the lectures) needs to be implemented for safety restrictions, else the design needs to incorporate force feedback (virtual or real) for safety.

## 2.5 Recommendations for Clinical Usage

The conclusion is that the distance sensor should be used with a virtual force feedback. It is suggested that the slave robot controller should be tuned towards a high resistivity, and operated slowly. The primary constraint is that the user must be aware of the location of the needle at all times. This is relatively self explanatory, as while the eyeball has several different regions of different densities, relying on the feedback "stiffness" is not sufficient. We propose that, if the operation is taken slowly, then a virtual force feedback can be simulated and felt by the operator. Slow operation could potentially help account for communication delays, as the difference in stiffness is region based. The exact amount of desirable resistance will depend on the operator, but should exceed  $K_p : K_d = 20 : 1$  for the slave controller, and  $K_p : K_d = 40 : 1$ .

## References

Beerens, R. (2017). *Bilateral teleoperation: controllers, time delays and performance*. Eindhoven University of Technology. [1]

D.J.F. Heck, Delayed Bilateral Teleoperation: a direct force-reflecting control approach, Ph.D. thesis, 2015 [2]

[https://brml.org/uploads/tx\\_sibibtex/Ped2008.pdf](https://brml.org/uploads/tx_sibibtex/Ped2008.pdf) [3]

<http://courses.shadmehrlab.org/Shortcourse/stiffness.pdf> [4]

[https://www.researchgate.net/publication/242415677\\_Estimated\\_versus\\_Calculated\\_Viscous\\_Friction\\_Coefficient\\_in\\_Spool\\_Valve\\_Modeling](https://www.researchgate.net/publication/242415677_Estimated_versus_Calculated_Viscous_Friction_Coefficient_in_Spool_Valve_Modeling) [5]

<https://www.ncbi.nlm.nih.gov/pmc/articles/PMC5623341/> [6]

<https://ieeexplore.ieee.org/document/7865997/> [7]